effects in the radiation patterns in the forearm direction are also observed as well, which are similar to the observations for the conventional internal mobile phone antennas [14-18].

ACKNOWLEDGMENTS

The generous support of Schmid & Partner Engineering AG (SPEAG) for SEMCAD-X simulation software is greatly appreciated.

REFERENCES

1. K.L. Wong, Planar antennas for wireless communications, Wiley, New York, USA, 2003.
2. Y.W. Chow, E.K. Ning Yung, K.F. Tsang, and H. T. Hui, An innovative monopole antenna for mobile-phone handsets, Microwave Opt Technol Lett 25 (2000), 119-121.
3. P.L. Teng and K.L. Wong, Planar monopole folded into a compact structure for very-low-profile multiband mobile-phone antenna, Microwave Opt Technol Lett 33 (2002), 22-25.
4. C.Y. Chiu, P.L. Teng and K.L. Wong, Shorted, folded planar monopole antenna for dual-band mobile phone, Electron Lett 39 (2003), 1301-1302.
5. K.L. Wong, G.Y. Lee, and T. W. Chiou, A low-profile planar monopole antenna for multiband operation of mobile handsets, IEEE Trans Antennas Propag 51 (2003), 121-125.
6. P.L. Teng, C.Y. Chiu, and K. L. Wong, Internal planar monopole antenna for GSM/DCS/PCS folder-type mobile phones, Microwave Opt Technol Lett 39 (2003), 106-108.
7. C.C. Lin, H.C. Tung, H.T. Chen, and K. L. Wong, A folded metal-plate monopole antenna for multiband operation of a PDA phone, Microwave Opt Technol Lett 39 (2003), 135-138.
8. S.Y. Lin, Multiband folded planar monopole antenna for mobile handsets, IEEE Trans Antennas Propag 52 (2004), 1790-1794.
9. T.K.W. Low, Z.N. Chen, and N. Yang, Bent planar monopole operating at GSM/ DCS/PCS/IMT2000 quad-bands, Microwave Opt Technol Lett 40 (2004), 170-172.
10. Y.S. Shin, S.O. Park, and M. Lee, A broadband interior antenna of planar monopole type in handsets, IEEE Antennas Wireless Propag 4 (2005), 9-12.
11. K.L. Wong, Y.W. Chi, and S. Y. Tu, Internal multiband printed folded slot antenna for mobile phone application, Microwave Opt Technol Lett 49 (2007), 1833-1837.
12. M. Francavilla, A. Schiavoni, P. Bertotto, and G. Richiardi, Effect of the hand on cellular phone radiation, IEE Proc Microwave Antennas Propag 148 (2001), 247-253.
13. O. Kivekas, J. Ollikainen, T. Lehtiniemi, and P. Vainikainen, Bandwidth, SAR, and efficiency of internal mobile phone antennas, IEEE Trans Antennas Propag 46 (2004), 71-86.
14. C.M. Su, C.H. Wu, K.L. Wong, S.H. Yeh, and C.L. Tang, User's hand effects on EMC internal GSM/DCS dual-band mobile phone antenna, Microwave Opt Technol Lett 48 (2006), 1563-1569.
15. C.H. Wu, K.L. Wong, C.I. Lin, C.M. Su, S.H. Yeh, and C.L. Tang, Simplified hand model including the user's forearm for the study of internal GSM/DCS mobile phone antenna, Microwave Opt Technol Lett 48 (2006), 2202-2205.
16. C.I. Lin, K.L. Wong, S.H. Yeh, and C.L. Tang, Study of an L-shaped EMC chip antenna for UMTS operation in a PDA phone with the user's hand, Microwave Opt Technol Lett 48 (2006), 1746-1749.
17. C.H. Wu and K.L. Wong, EMC internal GSM/DCS patch antenna for thin PDA phone application, Microwave Opt Technol Lett 49 (2007), 403-408.
18. C.I. Lin and K.L. Wong, Internal meandered loop antenna for GSM/DCS/PCS multiband operation in a mobile phone with the user's hand, Microwave Opt Technol Lett 49 (2007), 759-765.
19. http://www.semcad.com, SEMCAD, Schmid & Partner Engineering AG (SPEAG).
20. P. Vainikainen, J. Ollikainen, O. Kivekäs, and I. Kelander, Resonator-based analysis of the combination of mobile handsets antenna and chassis, IEEE Trans Antennas Propag 50 (2002), 1433-1444.

OPTIMIZATION OF POLYGONAL FRESNEL ZONE PLATES

Javier Alda[1] and Glenn Boreman[2]

[1] Applied Optics Complutense Group, University Complutense of Madrid, School of Optics, Av. Arcos de Jalón s/n., 28037 Madrid, Spain; Corresponding author: j.alda@opt.ucm.es

[2] CREOL, University of Central Florida, Orlando, FL 32816-2700

Received 16 July 2007

ABSTRACT: *The performance of Fresnel zone plates having polygonal boundaries between zones has been studied for polygons with a low number of sides. An optimized polygonal shape has been analytically defined by minimizing the mismatched area between the circular and the polygonal pseudo-Fresnel zones. The square polygon has been analyzed in more depth than the others because of its simple symmetry.* © 2007 Wiley Periodicals, Inc. Microwave Opt Technol Lett 50: 536–541, 2008; Published online in Wiley InterScience (www.interscience.wiley.com). DOI 10.1002/mop.23125

Key words: *Fresnel zone plates; diffractive optical elements; millimeter-wave*

1. INTRODUCTION

Fresnel zone plates (FZP) [1] are very useful additions in micro- and nano-photonic elements and devices [2]. They can be easily integrated as flat optical elements with focusing capabilities. The most common designs use circles to define the contours of the contiguous Fresnel zones. When the resolution of the fabrication techniques is comparable with the spatial dimensions of the Fresnel zones, the actual fabricated contours circles are jagged versions of the perfect circular pattern. For those cases, the study of polygons with a large number of sides has received attention [3, 4]. In this article, we are more interested in the analysis of FZP having polygonal contours with a low number of sides. Those cases may occur when the FZP needs to be fitted with elements or systems having a finite number of axes of symmetry: squares, hexagons, etc. In fact, square FZPs have been designed and tested in the past to compare their performance with the classical circular ones [2]. Some algorithms have been also developed to optimize the parameters of the square FZP [5]. In this article, we extend the analysis to the case of a regular polygon having an arbitrary number of sides, while emphasizing our interest and calculation for a polygon with a low number of sides. The performance of a given polygonal FZP is compared with a circular FZP having the same number of rings. As expected, we will see that this performance is better as the number of sides of the polygon increases.

Section 2 of the article presents the basis of the design procedure along with definitions of the important parameters and symmetries of the problem. Section 3 is devoted to the analysis of the results provided by a numerical simulation of the polygon elements within a scalar diffraction model, with special attention to the case of the square FZP. The conclusions of the article are described in Section 4.

2. GEOMETRICAL DESIGN

A FZP works by adding, blocking, or shifting in phase selected portions of the incoming wavefront that would otherwise interfere destructively. The increase in the irradiance obtained by the FZP is, to a first-order approximation, proportional to the square of the number of Fresnel zones included. However, losses caused by Fresnel reflection at the surface of the FZP surface, shadowing between adjacent zones, and departure from the initial design due

to fabrication tolerances all contribute to the degradation in performance of an actual device.

In this article, we are mainly interested in the performance when a polygon shape with a low number of sides replaces the classical circular shape of the FZP. Thus, the reference performance will be that of the circular FZP. In this analysis we will use the scalar diffraction model and a plane wave incidence as a basic approach. The calculation will include the effect of the obliquity factor. The Fresnel reflection losses will be assumed to be equal for the circular and polygonal cases, and thus will not be taken into account.

The radius of the contours of the circular Fresnel zones are characterized by the well known dependence,

$$R_m = \sqrt{f' \lambda_d m + \left(\frac{\lambda_d m}{2}\right)^2}, \tag{1}$$

where m is the order of the Fresnel zone, f' is the primary focal length of the FZP, and λ_d is the design wavelength in the medium after the FZP (assuming that the FZP focuses within that medium). A very useful approximation neglects the second term within the square root and provides the well-known dependence where the zone radius is proportional to $\sqrt{m}$. These values will serve as a reference when calculating the geometric parameters of the polygon element.

Our first objective is to optimize the fitting of the circular shape to a polygonal shape. The circle of reference for the zone m has a radius R_m, given by Eq. (1). The parameter for the polygonal shape will be the apothem, x, along with the number of sides, s. The optimum polygon contour should intersect the circle of reference at a position that overfills the circle of reference in some regions and underfills it in the rest. When analyzing regular convex polygons we may restrict the region of computation to an angular range determined by an apothem and the line joining the center of the polygon and the closest vertex to the apothem location. The angle subtended by these lines is

$$\alpha_{\text{pol}} = \frac{\pi}{s}, \tag{2}$$

where s is the number of sides of the polygon. The region of the polygon within this angular range has always the shape of a right triangle. There are $2s$ equal right triangles in a regular polygon having s sides. From Figure 1 we may see that the polygon shape intersects with the circular Fresnel zone reference only once on the contour side of this right triangle, at an angular position given by α_{int}. The location of this intersection is the main issue that needs to be properly solved. In a recent article, Minin et al. [5] proposed an optimization based on the reduction of the phase mismatch between the contribution to a given pseudo-Fresnel zone of a square polygon and an actual circular Fresnel zone. Our approach is based on the minimization of the area that overfills and underfills the circular angular sector when the polygon is traced. By reducing this area we decrease the number of Huygens wavelets that belong to the areas $A1$ and $A2$ in Figure 1. The extent of this mismatched area has the following analytical form,

$$A = A1 + A2 = R_m^2\left(\alpha_{\text{int}} - \frac{1}{2}\alpha_{\text{pol}}\right) + x^2\left(\frac{1}{2}\tan\alpha_{\text{pol}} - \tan\alpha_{\text{int}}\right), \tag{3}$$

where R_m is the radius of the circular boundary of the m Fresnel zone, x is the value of apothem of the regular polygon, and α_{int} is the angle that defines the intersection between the polygon and the

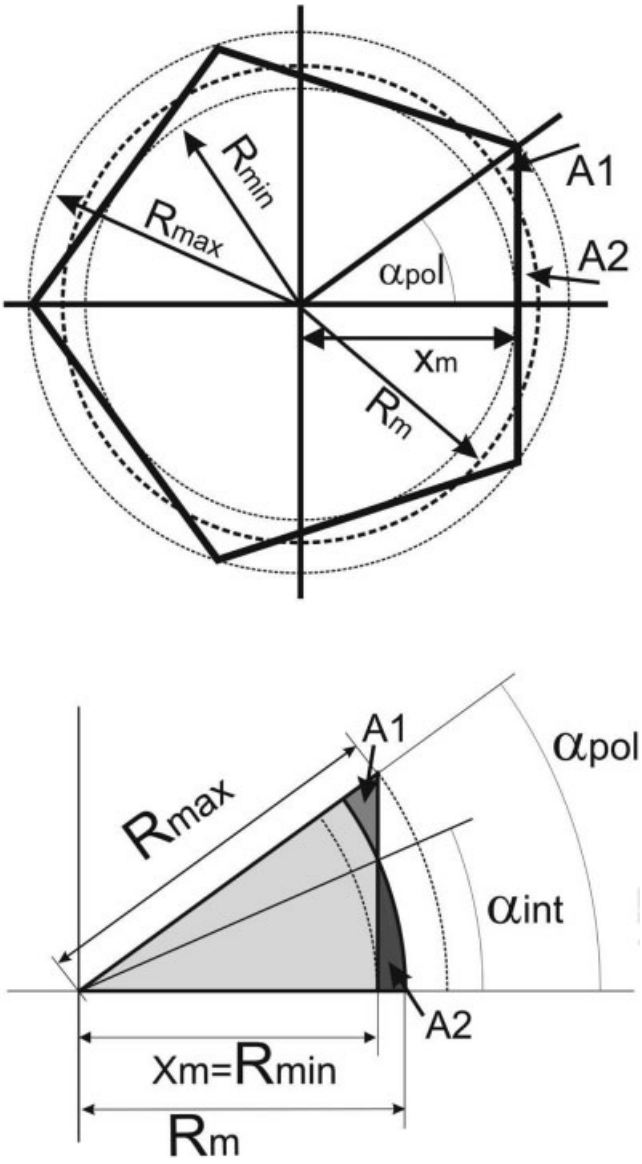

Figure 1 Geometric sketch of a pentagon ($s = 5$) fitted with the reference circular contour of radius R_m. The area that we try to minimize in the optimization procedure is the addition of $A1$ and $A2$. Angle α_{pol} is half the central angle of one of the sides of the polygon. Angle α_{int} defines the intersection between the polygon and circular contours. The dimension of the apothem is x_m. Also the dimensions of the minimum and maximum radius R_{min}, R_{max} intersected by the polygon contour are shown

circular contours (as seen in the lower portion of Fig. 1). This value can be related to the apothem value by the following relation,

$$\alpha_{\text{int}} = \cos^{-1}\frac{x}{R_m}. \tag{4}$$

By minimizing the total area, A, with respect to the value of the apothem, x, we find the optimized apothem value,

$$x_m = \frac{R_m}{\sqrt{1 + \dfrac{\tan^2(\pi/s)}{4}}}. \tag{5}$$

When the value of the optimized apothem, x_m, is normalized to the radius of the Fresnel zone, R_m, the result is independent of m and only depends on the number of sides, s, of the polygon. As a consequence of the Fresnel zone arrangement, the outer zones are more closely spaced. Then, it will eventually happen that a polygonal shape with a finite number of sides will intersect more than one circular Fresnel contour. This situation degrades the performance of the polygonal FZP and can only be avoided by limiting the number of allowed Fresnel zones for a given number of sides of the polygon.

Actually, for a given value of the apothem, the range of the circular shapes that can be intersected is given by the following two limits:

$$R_{\min}(x_m) = x_m, \tag{6}$$

$$R_{\max}(x_m) = \frac{x_m}{\cos\,\alpha_{\text{pol}}}, \tag{7}$$

These limits have been drawn in Figure 1. When the values given in Eqs. (6) and (7) are reached by the following or previous FZP radius, R_{m-1} or R_{m+1}, we know that another FZP circle is being intersected. It is interesting to note that the quotients $R_{\min}/R_m$, and $R_{\max}/R_m$, only depend on the number of sides of the polygon, s. We also know that a given m Fresnel zone is defined by two circular contours having an outer radius of R_m and an inner radius of R_{m-1}. The polygonal counterpart of this Fresnel zone is also defined by the corresponding apothem x_m (outer contour) and x_{m-1} (inner contour). The fitted polygonal contour involves, at least, the two adjacent and consecutive circular Fresnel zones. In the optimum situation these circular zones are the m, and $(m + 1)$ for the outer contour, and the $(m - 1)$ and m zones for the inner contour. Thus, we have a minimum of three circular Fresnel zones involved for each polygonal pseudo-Fresnel zone (there is a trivial exception with the central zone where the minimum number of involved circular Fresnel zones is 2). To describe this relationship, we define the following two conditions:

$$\frac{R_{m-2}}{R_{m-1}} \le \frac{R_{\min}}{R_0}, \quad \text{and,} \quad \frac{R_{\max}}{R_0} \le \frac{R_{m+1}}{R_m}, \tag{8}$$

where R_0 is the radius of the central Fresnel zone. The first condition avoids the intersection of the $m - 2$ circular contour (having a radius of R_{m-2}) with the inner polygon contour. The second condition avoids the intersection of the outer polygon contour of the zone with the next circular contour of order $m + 1$ (having a radius of R_{m+1}). Upon substitution of these values of $R_{\max}$ and $R_{\min}$ [Eqs. (6) and (7)] in the previous relations, we find that the upper limit involving $R_{\max}$ is the most demanding. This limit can be written as

$$m \le \frac{4}{3\tan^2\left(\frac{\pi}{s}\right)} + \frac{1}{3}. \tag{9}$$

This condition means that, for a FZP with polygon contours having s sides, there exist a limited number of pseudo-Fresnel zones, m, involving contributions of only the adjacent circular Fresnel zones. Above the zone order given by this condition, there will be four or more circular Fresnel zones contributing to one polygon pseudo-Fresnel zone. Figure 2 shows the line defining this limit. The optimum combinations of number of sides of the polygon contour, s, and number of zones, m, are located below the line. This inequality can be used to properly select a given polygon having s sides for a FZP having m Fresnel zones, or vice versa. This condition is somewhat less restrictive than the one calculated in [4] which is based in a value of the Strehl ratio equal to 0.8. In the next section, we will focus on the comparison of performance of the polygonal FZP compared with that of the circular FZP. For the sake of simplicity, we will only analyze the cases of square ($s = 4$), octagon ($s = 8$), and hexadecagon ($s = 16$). For these polygons, the maximum order of the zone satisfying the condition (9) is $m = 1$ for the square (only the central square fulfill the condition), $m = 8$ for the octagon, and $m = 34$ for the hexadecagon.

3. NUMERICAL SIMULATION

In this section, we have evaluated the Strehl ratio defined as,

$$S = \frac{I_{\text{polygon FZP}}}{I_{\text{circular FZP}}}, \tag{10}$$

where $I_{\text{polygon FZP}}$, and $I_{\text{circular FZP}}$ are the irradiances at the first focal point of the polygon and circular FZPs, respectively. The calculation uses a scalar diffraction approach to obtain the complex amplitude contribution of each zone at the location of the focal point of the FZP. The goal is to maintain an acceptable performance compared with that of a circular FZP. Figure 3 illustrates three different FZPs for three choices of polygon shape ($s = 4$,8, and 16, square, octagon, hexadecagon, respectively). In the top of Figure 3, we see the Strehl ratio (normalized to the circular FZP having the same number of zones) of a binary FZP (alternatively obscured and transparent) when the central zone is not obscured. The representation is made in terms of the number of zones involved in the design. The changes in value happens every two zones because the even zones are obscured. The central plot of Figure 3 is for a phase FZP where an additional phase difference of π between consecutive zones has been included. Finally, at the bottom of Figure 3 we have represented the relative performance of a polygonal contour phase FZP that has been specifically

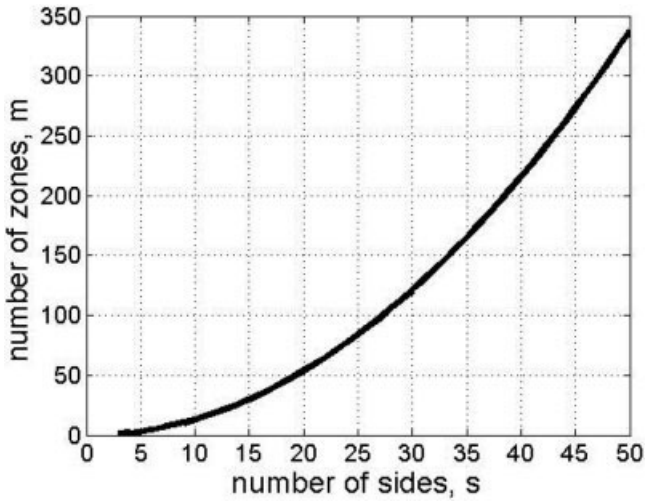

Figure 2 The minimum number of circular Fresnel zones intersected by a polygonal pseudo-Fresnel zone of order m is three (except for the first zone that will intersect only two). They are the $m - 1$, m, and $m + 1$ circular Fresnel zones. The line shown in this plot represents the dependence of the Fresnel zone number, m, with respect to the number of sides of the polygon, s that maintains this minimum number of intersected zones. The combinations of m and s above the curve involve more than three circular Fresnel zones

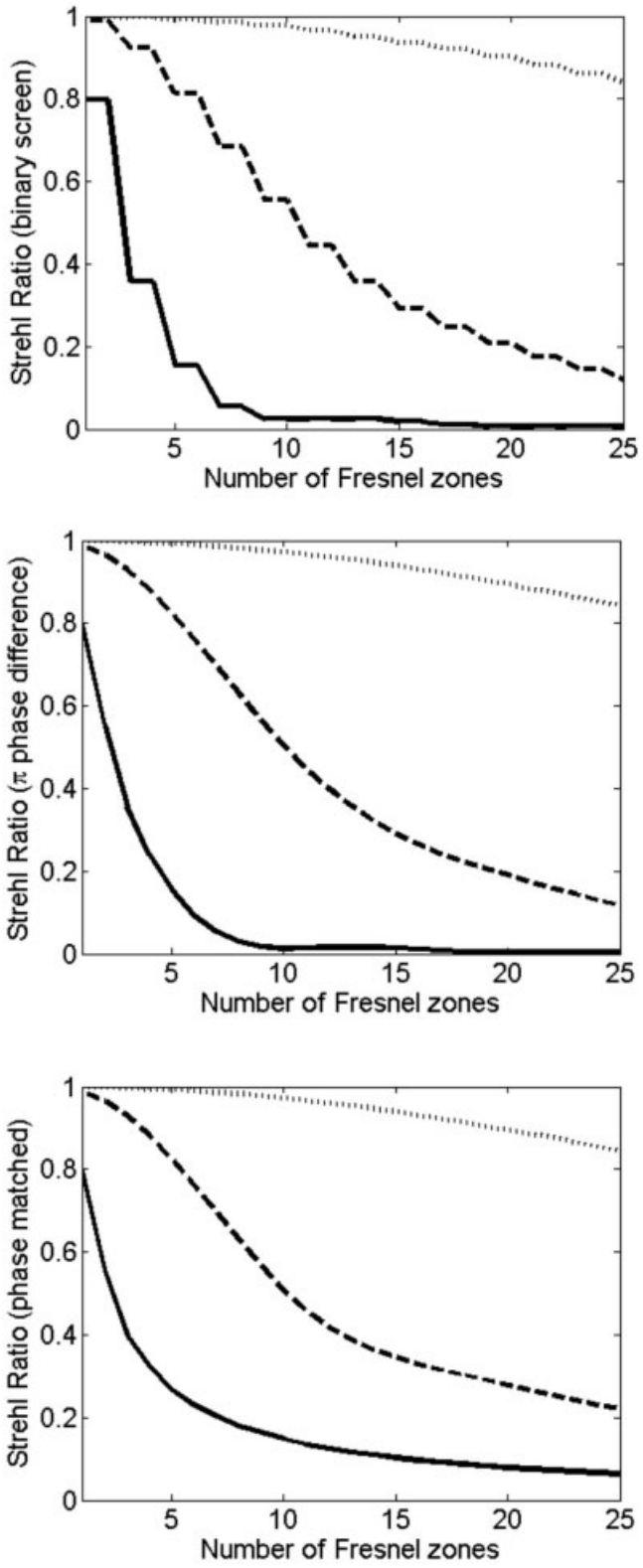

Figure 3 Strehl ratio for a binary FZP (top), a phase FZP with consecutive phase difference of π (medium), and a perfect phase matched FZP (bottom). The plots have been calculated for three polygonal shapes having $s = 4$ (solid), 8 (dashed), and 16 (dotted)

tailored to produce a phase shift at each zone that perfectly matches the phase shift difference between consecutive pseudo-Fresnel zones. For a polygon contour this phase difference is no longer π, as for the circular Fresnel zone, and it depends on the geometry and the order of the pseudo-Fresnel zone. We may think of this design as a perfectly phase-matched one. As expected, as the number of sides of the polygon increases, i.e., the polygon becomes a circle, the Strehl ratio approaches 1. At the same time, the performance degrades when increasing the number of involved zones for a given polygon shape. This is due to the limiting condition (9). For example, if we require a Strehl ratio better than 0.5, we cannot use more than 2 Fresnel zones for the case of a square polygon FZP, and no more than 10 zones for an octagon. A 16-sided polygon will perform with $S > 0.8$ for all the cases treated here having a maximum number of 25 zones. Although a Strehl ratio of 0.5 could be seen as a poor performance for imaging purposes, there are some other nonimaging applications where the interest is in irradiance collection rather than image quality.

We have also calculated the spectral performance by varying the value of λ around the wavelength of design λ_d. The results are shown in Figure 4. In those plots, we have represented the irradiance gain at the first focal point normalized to the irradiance gain for the circular FZP at the design wavelength and having 25 Fresnel zones (circles or polygons). This is the spectral version of the Strehl ratio defined in Eq. (10) modified in the following way,

$$S(\lambda) = \frac{I_{\text{polygon or circular FZP}}(\lambda)}{I_{\text{circular FZP}}(\lambda_d)}. \tag{11}$$

In the top of Figure 4, we have plotted $S(\lambda)$ for the circular FZP along with $S(\lambda)$ for the square, octagon, and hexadecagon. Again, as the number of sides grows the spectral behavior of the polygon is closer to the one of the circular FZP. The polygon spectral variation is smoother than for the circular FZP. This advantage is obtained by accepting a lower irradiance gain at the focal point.

3.1. The Square FZP

The square FZP design is an appealing arrangement for fabrication. We have seen previously that the behavior of the square polygon is not as good as the one obtained with circles [2]. However, the phase variation between successive square Fresnel zones optimized follows a regular pattern. This makes easier to define a phase profile that adds in phase all the contributions from the square zones. In Figure 5, we have represented the profile of the phase screen that would do this perfect matching of the phase for a transmissive element having a focal length of 10 mm, for a wavelength of 500 nm, and a material having an index of refraction of 1.5. We may verify that after the first Fresnel zone, the rest of the zones can be grouped in 5 levels that repeat themselves along the FZP with a consecutive phase difference of $2\pi/5$. This periodic pattern is due to the special relations that arise from the selection of the optimum size for the value of the apothem of the square. The point of intersection between the circular contour and the optimized apothem of the square is defined by an angle $\alpha_{\text{int}} = \cos^{-1}(2/\sqrt{5})$. If we generalize this equation to obtain the intersection of the circular contour having radius R_m [see Eq. (1)], with the square having an apothem $x_{m'}$ [see Eq. (5)], we find that the intersection point is given by

$$\alpha_{\text{int},m,m'} = \cos^{-1}\left(\sqrt{\frac{4m'}{5m}}\right). \tag{12}$$

When m and m' are both allowed to vary, we see that for every 5 square contours there exists a situation where two circular contours act as the inscribing circle, ($\alpha_{\text{int},,m,m'} = 0$) and circumscribing circle ($\alpha_{\text{int},,m,m'} = \pi/4$) for the square. This happens for $m' = 5$,

10, 15, . . . As far as the ratio between the circular and square zones depends on m and m', the extent of mismatched area follows a periodic pattern that repeats itself every 5 zones. This mismatched area is responsible for the overall phase of the square zone maintaining the periodic phase pattern.

By using the phase profile shown in Figure 5, a square FZP with 25 zones would have an ideal irradiance gain at the focus of about 160, instead of 16 that would result from a binary square FZP with 25 zones. The spectral variation of the perfectly-matched square FZP is shown in the bottom plot of Figure 4. We see that the general shape of the curve resembles the one for the circular FZP, but at a lower level.

On the other hand, when representing the increase in irradiance at the focal point of the perfectly phase-matched square FZP, we find that the dependence is linear with the number of zones. This result opens the way for trade studies for the use of square FZP, where this linear dependence is the price paid for having rectangular symmetry.

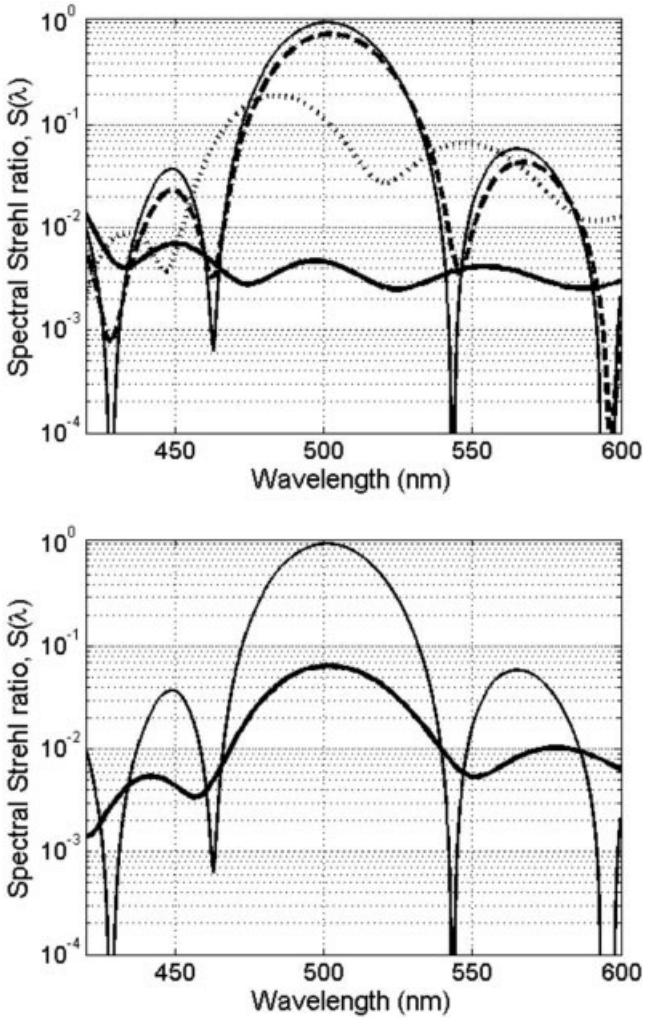

Figure 4 Semilog plot of the spectral Strehl ratio, $S(\lambda)$, for polygon and circular FZPs having 25 pseudo-Fresnel zones for the polygon case, and 25 Fresnel zones for the circular case. The plot in the top represents $S(\lambda)$ for three polygons having 4 (thick solid line), 8 (dashed line) and 16 (dotted line) sides. The plot at the bottom represents $S(\lambda)$ of a perfectly phase-matched square FZP having 25 pseudo-Fresnel zones (thick solid line). $S(\lambda)$ for the circular FZP is plot as a thin solid line in both plots

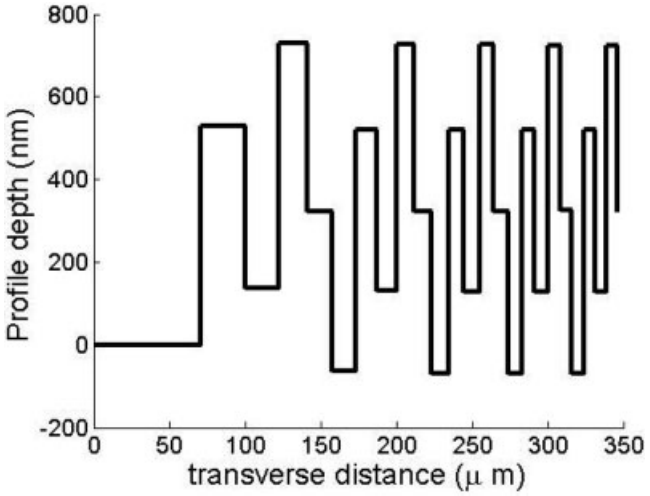

Figure 5 Plot of the transverse profile for a phase screen that would perfectly match all the phase shifts of the square FZP. It should be noted that the aspect ratio of this profile is highly exaggerated because the depth is represented in nm meanwhile the transverse distance is given in microns

4. CONCLUSIONS

Considering polygonal zone plates, we have optimized the designs by minimizing the circular area overfilled and underfilled by the polygon. For the case of a square polygon, the optimized polygon is very similar to the one obtained recently by other authors, and differs significantly from the one used by the authors in a previous article. We have evaluated the performance of polygonal diffractive elements that could be used instead of the classical circular FZP.

The results obtained here quantify the constraints and performance of the polygonal designs. As expected, the polygonal designs perform better as the number of sides of the polygon increases. However, for a limited number of Fresnel zones, the polygon performance is not strongly affected by the polygon shape. Because of the special symmetry of the square polygon, we have investigated the improvement of the square FZP obtained by including a customized phase screen that adds the right phase in order to have a perfect phase matching. The diffractive increase of the irradiance for this case is linear with the number of square Fresnel zones, instead of parabolic as for the circular Fresnel zones.

ACKNOWLEDGMENTS

This work has been done during a stay of Dr. Alda at CREOL (University of Central Florida). This stay has been funded by the Ministerio de Educación y Ciencia of Spain under the Program for the Mobility of Spanish Researchers (PR2006-0006) and by a grant from CREOL. This work has been also partially funded by the Research Project TEC2006-1882 from the Ministerio de Educación y Ciencia of Spain.

REFERENCES

1. H. D. Hristov, Fresnel zones in wireless links, zone plate lenses and antennas, Artech House Ed, Norwood, MA (USA), 2000.
2. F.J. Gonzalez, J. Alda, B. Ilic, and G. Boreman, Infrared antennas coupled to lithographic Fresnel zone plates, Appl Opt 43 (2004), 6067–6073.
3. I. Kallioniemi, J. Saarinen, K. Blomstedt, and J. Turunen, Polygon approximation of the fringes of diffractive elements, Appl Opt 36 (1997), 7217–7223.

4. Z. Chen, Y. Vladimirsky, M. Brown, O. Vladimirsky, F. Moore, F. Cerina, B. Lai, W. Yun, and E. Gluskin, Design and fabrication of Fresnel zone plates with large numbers of zones, J Vac Sci Technol B 15 (1997), 2522–2527.
5. I.V. Minin, O.V. Minin, A. Petosa, and S. Thirakuone, Improved zoning rule for designing square fresnel zone plate lenses, Microwave Opt Technol Lett 49 (2007), 276–278.

A SMALL DIE AREA AND WIDE LOCKING RANGE CMOS FREQUENCY DIVIDER

Sheng-Lyang Jang, Jui-Cheng Han, Chien-Feng Lee, and J.-F. Huang
Department of Electronic Engineering, National Taiwan University of Science and Technology, 43 Keelung Road, Section 4, Taipei, Taiwan 106, Republic of China; Corresponding author: sljjj@mail.ntust.edu.tw

Received 21 June 2007

ABSTRACT: *This letter proposes a new injection-locked frequency divider (ILFD) with wide locking range and small die area. The proposed CMOS ILFD consists of an injection MOS and an LC tank voltage-controlled oscillator with a cross-coupled switching pair and tunable active inductors. The divide-by-2 ILFD was fabricated in the 0.18-μm 1P6M CMOS technology. At the supply voltage of 1.8 V, the divider free-running frequency is tunable from 1.46 to 2.7 GHz, and at the incident power of −4 dBm the locking range is about 3.4 GHz (79%), from the incident frequency of 2.6 to 6.0 GHz. The core power consumption is 7.2 mW and the die area is 0.383 × 0.379 mm².* © 2007 Wiley Periodicals, Inc. Microwave Opt Technol Lett 50: 541–544, 2008; Published online in Wiley InterScience (www.interscience.wiley.com). DOI 10.1002/mop.23090

Key words: *CMOS; injection-locked frequency divider; locking range; tunable active inductor*

1. INTRODUCTION

With the increasing demands on high data-rate communication services, the development of high-speed mixed signal integrated circuits has attracted great attention in recent years. As one of the key components in high-speed systems, the frequency divider (FD) is widely used for applications in frequency synthesizers and signal generator. FDs take a periodic input signal and generate a periodic output signal at a frequency that is a fraction of the input signal. There are several existing topologies for FD such as current-mode logic (CML) [1], dynamic logic [2] and injection-locked oscillators, and Miller divider [3]. The circuit topologies in Refs. 1 and 2 use two differential amplifier stages, while the injection-locked FD (ILFD) [4] and Miller divider utilize one differential stage, the latter circuits are potential for low power application. For high-speed operation, the FD utilizing an LC resonator is the most suitable one among various types of FDs [5], because the operating frequency is determined by the resonant frequency. However, the locking range of conventional LC-resonator divider is generally narrow, the operation margin is small, and the process variation may cause operation failure.

In this paper, we propose a new ILFD with small die area for low cost application and wide locking range to cope with process variation. The proposed ILFD uses active inductors rather than passive inductors to reduce the production cost and the system dimension. At low gigahertz range, using a passive inductor results in a large chip area and increase in the cost of the product. The use of active inductor can lower the product cost; however, there are three major products. The use of active inductor can lower the product cost; however, there are three major drawbacks [6] in using active inductors, these are the limited operation frequency range, higher noise figure, and large dc power consumption. The proposed tunable active inductor (TAI) ILFD can avoid these drawbacks. First, the active inductor is tunable; therefore, the locking range is extended by the tuning mechanism. Second, the phase noise performance of ILFD is determined primarily by external low-phase noise injection source. Finally, the power consumption is controlled by a tail transistor. The proposed ILFD has a locking range from 2.6 to 6.0 GHz and was implemented in a 0.35-μm CMOS process.

2. CIRCUIT DESIGN

The operating principle of the TAI and the ILFD is discussed in this section. The implementation of TAI is based on the gyrator-C architecture including a gain and a feedback element. The circuit schematic of the fully TAI is shown in Figure 1(a). The TAI consists of two transistors generating inductive impedance, and it occupies a very small die area. Transistors Mp and Mn are used as current sources, while M1 and M2 form the gyrator. Conventionally, the so-called cascode-grounded active inductor, by adding a transistor M3 stacked on top of M1 in Figure 1(a) [7], is used to form a TAI. The cascode-grounded active inductor with three stacked MOSFETs is not used here since it requires larger voltage headroom. The two-stacked-MOSFETs TAI topology is adopted for low voltage implementation. To gain design insight of the TAI, we propose a mathematical circuit model for the TAI. The equivalent small-signal circuit of Figure 1(a) is shown in Figure 1(c), which can be treated a simplified LC tank circuit shown in Figure 1(b). In Figure 1(c), g_{dp} and g_{dn} are the drain conductance of Mp

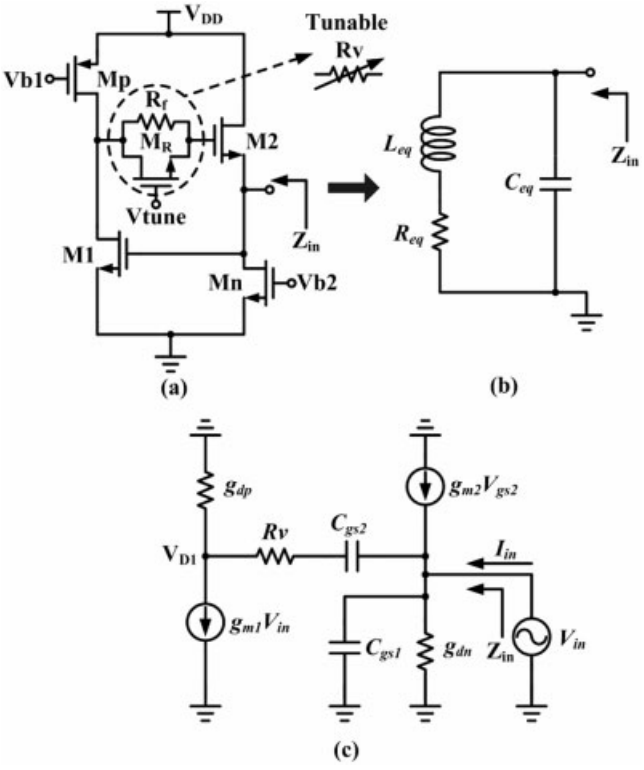

Figure 1 Schematic of the tunable active inductor circuit and its equivalent model